AIP | Review of Scientific Instruments

A liquid jet setup for x-ray scattering experiments on complex liquids at free-electron laser sources

I. Steinke, M. Walther, F. Lehmkühler, P. Wochner, J. Valerio, R. Mager, M. A. Schroer, S. Lee, W. Roseker, A. Jain, M. Sikorski, S. Song, R. Hartmann, M. Huth, L. Strüder, M. Sprung, A. Robert, P. H. Fuoss, G. B. Stephenson, and G. Grübel

Citation: Review of Scientific Instruments **87**, 063905 (2016); doi: 10.1063/1.4953921
View online: http://dx.doi.org/10.1063/1.4953921
View Table of Contents: http://scitation.aip.org/content/aip/journal/rsi/87/6?ver=pdfcov
Published by the AIP Publishing

A liquid jet setup for x-ray scattering experiments on complex liquids at free-electron laser sources

I. Steinke,[1,2] M. Walther,[1] F. Lehmkühler,[1,2,a)] P. Wochner,[3] J. Valerio,[1] R. Mager,[4] M. A. Schroer,[1,2] S. Lee,[5] W. Roseker,[1] A. Jain,[1] M. Sikorski,[6] S. Song,[6] R. Hartmann,[7] M. Huth,[7] L. Strüder,[7] M. Sprung,[1] A. Robert,[6] P. H. Fuoss,[8] G. B. Stephenson,[8] and G. Grübel[1,2]

[1]*Deutsches Elektronen-Synchrotron (DESY), Notkestr. 85, 22607 Hamburg, Germany*
[2]*The Hamburg Centre for Ultrafast Imaging (CUI), Luruper Chaussee 149, 22761 Hamburg, Germany*
[3]*Max Plank-Institut für Festkörperforschung, Heisenbergstr. 1, 70569 Stuttgart, Germany*
[4]*Max Plank-Institut für Intelligente Systeme, Heisenbergstr. 3, 70569 Stuttgart, Germany*
[5]*Frontier in Extreme Physics, Korea Research Institute of Standards and Science (KRISS), Daejeon 305-600, South Korea*
[6]*LCLS, SLAC National Accelerator Laboratory, Menlo Park, California 94025, USA*
[7]*PNSensor GmbH, Sckellstraße 3, 81667 München, Germany*
[8]*Argonne National Laboratory, Argonne, Illinois 60439, USA*

(Received 8 March 2016; accepted 1 June 2016; published online 17 June 2016)

In this paper we describe a setup for x-ray scattering experiments on complex fluids using a liquid jet. The setup supports Small and Wide Angle X-ray Scattering (SAXS/WAXS) geometries. The jet is formed by a gas-dynamic virtual nozzle (GDVN) allowing for diameters ranging between 1 μm and 20 μm at a jet length of several hundred μm. To control jet properties such as jet length, diameter, or flow rate, the instrument is equipped with several diagnostic tools. Three microscopes are installed to quantify jet dimensions and stability *in situ*. The setup has been used at several beamlines performing both SAXS and WAXS experiments. As a typical example we show an experiment on a colloidal dispersion in a liquid jet at the X-ray Correlation Spectroscopy instrument at the Linac Coherent Light Source free-electron laser. *Published by AIP Publishing.* [http://dx.doi.org/10.1063/1.4953921]

I. INTRODUCTION

The recent advent of modern synchrotron and X-ray Free Electron (XFEL) light sources allows studying structure and dynamics of soft condensed matter with unreached spatial and temporal resolution. In particular, the short x-ray pulse duration and the high degree of coherence of XFEL beams[1–3] enable new types of experiments such as particle imaging[4–6] or correlation studies.[7–11]

In such FEL experiments liquid jet injection systems are often used as sample delivery for several reasons. Most importantly, a jet is a fast steady stream injection system that refreshes the sample permanently. In conventional sample environments for liquid samples such as capillary containers, the accumulated x-ray dose frequently leads to extensive sample damage.[9,10,12,13] Thus, x-ray scattering experiments on radiation sensitive samples such as protein complexes are often performed with steady streaming liquid jets.[4–6] For this purpose different setups are used for x-ray scattering experiments on liquid jets at modern x-ray sources.[14–19] Typically, these systems are permanently installed at dedicated beamlines.

In this paper we describe the design and performance of a liquid jet setup, which is dedicated to Small Angle X-ray Scattering (SAXS) as well as Wide Angle X-ray Scattering (WAXS) experiments. The setup is designed to be used at different x-ray beamlines. The jet can be monitored by three microscopes. In this way we are able to measure *in situ* the length and diameter of the jet and the size of the droplets that form at the end of the liquid jet. In particular, the setup is compatible to vacuum chambers of cooled detector systems via a differential pumping stage and allows thus x-ray diffraction experiments on molecular liquids. First experimental results from a WAXS experiment on a jet formed from a colloidal dispersion performed at the X-ray Correlation Spectroscopy (XCS) instrument at the Linac Coherent Light Source (LCLS) are discussed.

II. LIQUID JET SETUP

Figure 1(a) shows a CAD drawing of the liquid jet chamber indicating its overall dimensions. The sample chamber comprises various parts, such as vacuum pumps, microscopes for *in situ* observation, and diagnostics of the liquid jet and a nozzle holder with various diagnostics tools. The total weight of the chamber is 120 kg. It is balanced in order to be mounted on any diffractometer sample table that is capable of supporting the weight. The x-ray beam direction is given by the red arrow. Three different microscopes are mounted on the chamber to record images of the jet from different directions. Figure 1(b) shows a detailed view of the microscope setup. Custom-made nozzles are mounted on a holder which can be moved in all three directions by high-resolution stepping motors. Gas-dynamic virtual nozzles (GDVN)[20–24] are used to inject the liquid as typically used in state-of-the-art experiments. Here, a gas streams coaxially around the liquid to compress and form the liquid jet. This technique allows producing liquid jets of diameters down

a)Electronic mail: felix.lehmkuehler@desy.de

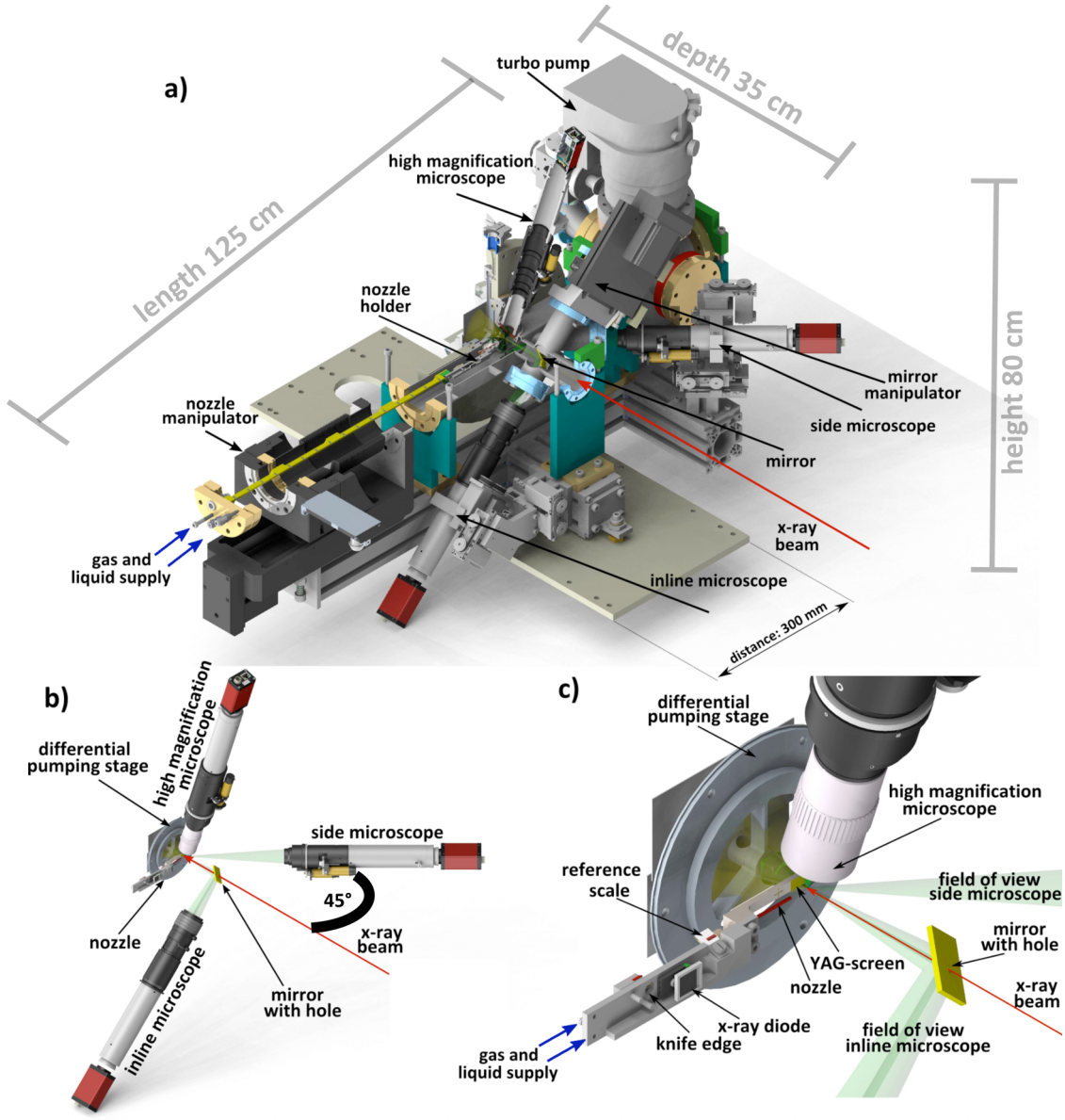

FIG. 1. (a) Overview of the liquid jet setup showing nozzle holder, manipulators, and microscopes. (b) Detailed arrangement of the microscopes. (c) Close up of the nozzle holder. The differential pumping stage was used for WAXS experiments at LCLS.

to the μm regime at flow rates of 5 to 15 μl/min. After a few hundred μm, the jet typically breaks up into a train of droplets. Optionally, a piezo motor (SmarAct) can be installed at the nozzle holder to achieve a sub-μm resolution in height. In Fig. 1(c) a close up of the nozzle holder including the nozzle and other diagnostics, e.g., a knife edge for beam size determination and a fluorescence screen for determination of the beam position, is shown.

For the liquid and gas supply to the GDVN, two feedthroughs are placed at the entrance of the manipulator, depicted by the blue arrows at the entrance of the nozzle manipulator in Fig. 1(a). The liquid flow is measured outside of the chamber using a micro-flow meter (Sensiron AG, SLG1430). The gas and liquid pressures are controlled by high precision valve regulators (ProportionAir, GP1 series). Using these devices the gas and liquid pressures are controlled with an accuracy of 0.1% between $p_{\min} = 0.4$ bar and $p_{\max} = 68.9$ bar.

The three microscopes are used to observe the size and alignment of the jet *in situ*. These are an inline microscope to control the jet in beam direction, a high magnification microscope to measure jet and droplet sizes, and a side microscope mounted at 45° with respect to the beam direction. All microscope objectives in the setup are equipped with universal compact cameras (Allied Vision, Manta G-146B). These offer recording up to 17 Hz using a CCD with 1388×1038 pixels. The exposure time of the cameras can be as short as $t_e = 31$ μs. Since liquid jets are visible best when back-illuminated, custom-made pulsed light sources using Light Emitting Diodes (LEDs) are installed opposite to each microscope objective (not shown in Figure 1) to ensure that each microscope can look across the jet and directly into a LED. The sensitivity of the CCD is the highest for green light, thus 0.5 W LEDs emitting at $\lambda = 510$ nm were used with pulse lengths down to 50 ns at repetition rates up to 120 Hz. Typically, we use a repetition rate of

10 Hz and pulse lengths of 200 to 400 ns for the high magnification microscope and 100 μs for the inline and side microscope. The focus and the zoom of all microscope objectives are motorized using high resolution stepping motors.

The inline microscope is a 12× macro-zoom-objective (Navitar, Zoom-Motorized Lenses) in combination with an ancillary lens (Navitar, Lens Attachments). In this configuration the objective allows a magnification up to 7 times at a focal distance of d_f = 165 mm. In this setting, a maximum reachable resolution of the recorded images of $\Delta \approx 0.67$ μm/pixel can be achieved but it is limited by the objective to about 6.6 μm.

The size of the jet and droplets can be measured using the high magnification microscope. The microscope consists of a high resolution 12× microscope objective (Navitar, UltraZoom-Motorized Lenses) and a high magnification ancillary lens (Mitutoyo 10X). It allows recording microscope images at a focal distance of d_f = 33 mm and a magnification factor up to 66. Images can be recorded at a theoretical resolution of $\Delta \approx 0.07$ μm/pixel, but it is limited by the resolution error of the objective ($R_E = \pm 0.9$ μm). Its resolution can be calibrated *in situ* with the reference scale mounted on the nozzle holder (see Fig. 1(c)). Since the flow velocities of the droplets are in the order of several m/s, microscope images have to be recorded at short exposure times to access a quasi-static image of the droplets. Thus, the exposure time of the high magnification microscope is reduced using a stroboscopic back-illuminating light source with a pulse duration of up to 400 ns.

For checking the liquid flow and the stability of the jet, a side microscope is mounted in the setup. Furthermore, the side microscope allows an *in situ* control of the jet because the LED for the inline microscope has to be moved out from the beam path during the experiment. Thus, using the LED from the side microscope, the inline microscope can also be used in reflection geometry when its back-illuminating diode has been removed. The side microscope offers a view on the tip of the nozzle under 45° in the horizontal plane with a magnification factor up to 4.5 times at a focal distance of d_f = 175 mm, see Figure 1(b). It consists of a macro-zoom-objective (Navitar, Zoom 6000-Motorized Lenses) and an ancillary lens (Navitar, Lens Attachments). The microscope images recorded with the side microscope having a theoretical resolution of $\Delta \approx 1$ μm/pixel which is limited by the objective to about 9.5 μm.

The alignment of the jet to the X-ray beam is performed using the inline microscope. In order to visualise the liquid jet, a mirror is moved to the beam path that reflects the light from the LED source by 90° to the inline microscope. The X-ray beam can pass the mirror through a hole of 2 mm diameter. This mirror can be translated in two dimensions using the mirror manipulator with a high resolution stepping motor (Oriental Motors, PK268.4-E2.0B) and a piezo motor (SmarAct), see Figure 1(a). To define the X-ray beam position, a fluorescence screen made from Yttrium-Aluminium-Garnet (YAG) is used. This screen is mounted on the nozzle holder (see Figure 1(c)) and moved to the beam position before the experiment. After the beam position has been marked on the microscope display the jet is moved back to the desired X-ray beam position.

The entrance of the setup consists of a CF40 flange while the exit is a custom made flange. Exit flanges allowing SAXS, combined SAXS/WAXS and WAXS experiments are available. Thus the setup can be connected to standardized vacuum components of a beamline. Vacuum conditions at $p_{vac} = 10^{-6}$ mbar without and $p_{vac} = 10^{-3}$ mbar with a running jet are ensured by using three different vacuum pumps (roughing pump (Edwards, XDS35i), booster pump (Edwards, XDS100B), turbo pump (Pfeiffer, HiPace 300P)). The vacuum pressure p_{vac} is measured by three Ceramic Capacitance Gauges (Pfeiffer Vacuum, CMR 365, CMR 364, CMR 363). These gauges enable measurements between $p_{vac} = 10^{-5}$ mbar and $p_{vac} = 11$ mbar with an accuracy of 0.5% independently of the gaseous atmosphere inside of the chamber. Since a GDVN injects liquid and helium, the use of such gas independent gauges is necessary. For additional measurements of the pressure a full range gauge (Pfeiffer Vacuuum PKR 261) is used. Its sensitive range of operation is between $p_{vac} = 10^{-9}$ mbar and $p_{vac} = 1000$ mbar at an accuracy up to 30%, dependent on the pressure of the gaseous atmosphere inside the chamber.

Besides the characterization of the jet, diagnostic tools are installed to characterize the x-ray beam during an experiment. The intensity of the direct x-ray beam can be measured using an x-ray diode (Hamamatsu S3590-09) that is mounted on the nozzle holder, see Fig. 1(c). Thus, intensity measurements can be performed without breaking the vacuum or disturbing the jet. Furthermore, on the nozzle holder a knife edge is mounted to measure the beam size at the jet position.

III. EXPERIMENT

The liquid jet setup has been successfully used in experiments at the cSAXS beamline of the Swiss Light Source (SLS) at the Paul-Scherrer-Institute and beamline P10 at PETRA III (DESY), both in SAXS geometry, and at the XCS instrument[25] of the LCLS in WAXS geometry. Here we will concentrate on the demonstration experiment on spindle-shaped hematite particles in water performed at XCS. The setup was used in combination with a pnCCD-detector.[18,26,27] In Figure 2 a sketch of the geometry of the experiment is shown. The detector consists of two separated panels, which can be passed by the direct x-ray beam (green arrow). The jet-to-detector distance was d = 50 mm to access wide x-ray scattering signals from scattering angles θ = 17.4° to θ = 36°, that corresponds to wave vector transfers $q = \frac{4\pi}{\lambda}\sin(\theta/2)$ between q = 1.3 Å^{-1} and q = 2.8 Å^{-1} at an X-ray energy of $E_{x\text{-ray}} = 8.4$ keV. A self-seeded beam was used[28] in combination with the instrument's Si(111) double-crystal monochromator. The beam size was focused by compound refractive lenses to 5×3 μm^2 (h × v). In this configuration, the q-resolution was $\Delta q = 0.0015$ Å^{-1}.

As the vacuum condition inside the detector chamber was $p_{vac} = 10^{-8}$ mbar and in the sample chamber $p_{vac} = 10^{-3}$ mbar due to the injection of the sample dispersion, a differential pumping stage was used to compensate for the pressure

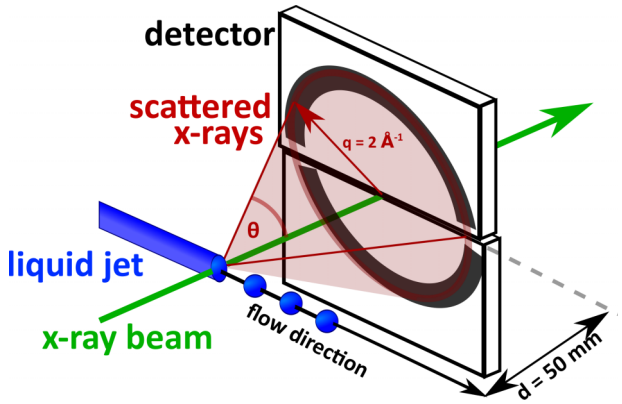

FIG. 2. Sketch of the scattering geometry showing the liquid jet with the detector panels.

difference, see Figure 1(c). The diameter of the stage is 72.6 mm with a center hole of inner diameter $d_i = 40$ μm allowing the x-ray beam to pass. Since the detector is sensitive to visible light, a black polyimide foil is used to separate the light emitted by the LEDs inside the vacuum chamber and the detector. The foil is glued on three supports that are directed from the center to the edges of the differential pumping stage.

As sample we used spindle-shaped hematite particles dispersed in water at a concentration of $c = 0.1$ vol. %. Its synthesis was described by Ozaki and co-workers.[29] The size of the particles was determined to about 80×320 nm^2 from SAXS patterns measured at the cSAXS beamline of SLS. The single crystalline colloidal particles exhibit a trigonal crystalline structure of hematite (space group $R\bar{3}c$).[30] Such spindle-shaped colloidal particles are known to be sensitive to shear flows by aligning to a preferred direction.[31] Thus, this sample system can be used to study the shear flow of a liquid jet.

In the experiment the jet was stable over at least each single experimental shift, i.e., more than 10 h. The jet diameter was measured with the high magnification microscope to $d_{\text{jet}} = (3.6 \pm 0.9)$ μm. The observed droplet diameter d_{drop} at the break up point varied between 5 μm and 8 μm. The break up length of the liquid jet was measured from several snapshots to be $L = (230 \pm 26)$ μm. The error is estimated from the standard deviation of the measurements. The difference between jet and droplet size and the break-up length corresponds to earlier observations of GDVN and Rayleigh jets.[23,32,33] The flow rate of the jet was about $Q \approx 11.4$ μl/ min at a vacuum pressure of $p_{\text{vac}} = 10^{-3}$ mbar.

Microscope images of the nozzle with liquid jet are shown in Figure 3. Here, the inline microscope was used in reflection geometry, i.e., its back-illuminating diode was moved away using the light from the side microscope's LED light. Due to the different curvature of the jet compared to the droplets, they reflect the light into the inline microscope camera differently (Figure 3(a)). Thus, the jet appears as a dark line in front of the nozzle tip, while the droplets appear as a bright line at the break up point. Because of the long exposure time of $t_e = 100$ ms, the droplets are smeared out in the microscope image. For the side microscope, the flow direction is out of plane and the depth of focus of the microscope objective is about $d_f = 20$ μm (Figure 3(b)). Thus, the first part of the jet at the nozzle tip is visible, while the rest of the jet is out of focus. The image taken with the high magnification microscope is shown in Figure 3(c). The exposure time was reduced using the stroboscopic light source to $t_e = 400$ ns. The image shows the jet and droplets that are formed due to the jet break up. The flow velocity $v = 18.7$ ms^{-1} can be calculated out of the measured jet diameter d and the measured flow rate Q. Within the exposure time t_e, the droplets cover a distance $\Delta x = 7.5$ μm. Since this value is comparable to the droplet diameter, the droplets appear smeared along the flow direction, see Figure 3(c).

In Figure 4 an average of approximately 37 000 single shot diffraction patterns recorded on the sample is shown. The pattern was corrected for dark images and for comparison, the intensity was normalized to the average value for each of the total of 16 ASICS of the pnCCD. Further corrections and analysis, e.g., taking into account background signals and common-mode corrections,[34] and a so-called droplet algorithm[35,36] to extract clean intensity values will be discussed in a subsequent publication. The pattern shows a bright scattering ring at $q = 2$ Å^{-1}, reflecting the first structure factor peak of liquid water.[37] At higher wave vector transfer q azimuthal segments of higher intensity are visible. These signals are related to the Bragg reflections from the hematite crystal structure of the colloids. The strongest signals can be assigned to the crystal planes (104) and (110) of the trigonal structure. Since only incomplete Debye-Scherrer rings are visible, an alignment of the spindle-shaped particles in flow direction is suggested. This alignment is in line to the results of other studies of elongated particles in flow.[31,38] The detailed particle alignment will be described in a subsequent publication.

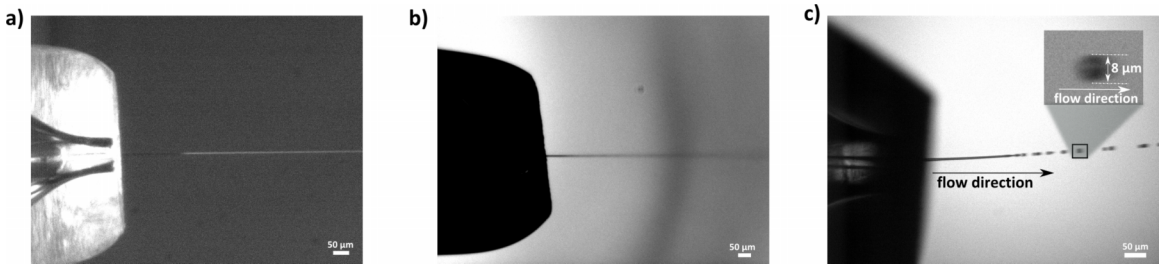

FIG. 3. Three microscope images of the liquid jet. The nozzle is located at the left side of each image and the jet is injected from the left to the right side. Microscope images were taken with: (a) inline microscope (reflection-illuminated, $t_e = 100$ ms), (b) side microscope (back-illuminated, $t_e = 50$ μs), (c) high magnification microscope with back-illuminating stroboscopic light ($t_e = 400$ ns). The inset shows a magnification in order to determine the droplet size.

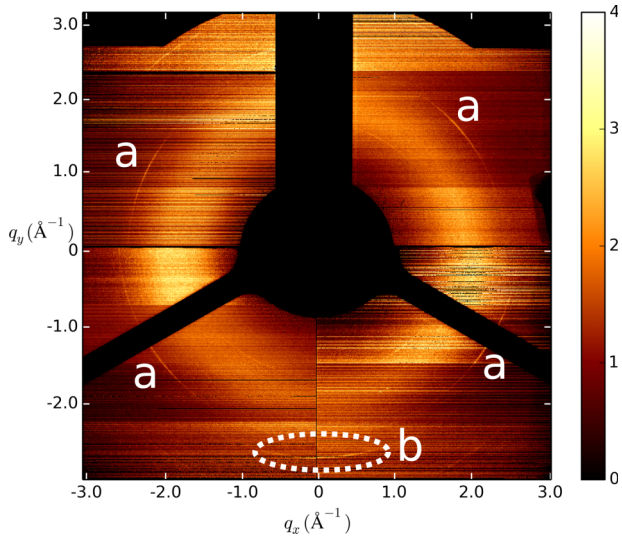

FIG. 4. Average of approximately 37 000 single shot diffraction patterns taken on the liquid jet. The shadows arise from the coverage of the differential pumping stage in front of the CCD chips. Intensity is given in arbitrary units. The hematite Bragg reflections are labeled as (a) (104) reflections and (b) the (110) reflection. Due to the differential pumping stage, the (110) reflection is only visible at the lower part of the detector. Further weak reflections can be assigned to parasitic scattering from the pumping stage. Note that the q-scale is different for the upper and lower part of the detector because of the offset of the panels.

IV. SUMMARY AND OUTLOOK

A liquid jet setup has been developed and adapted for WAXS and SAXS experiments. It has successfully been used at the cSAXS beamline at SLS, P10 of PETRA III, and the XCS instrument at the LCLS. Since the entrance of the setup consists of standardized vacuum components, it can be connected to any XFEL or storage ring beamline using a custom made exit flange. With a running jet, the pressure in the chamber is below $p_{vac} = 10^{-3}$ mbar. A differential pumping stage was developed to connect the setup to the pnCCD detector for the WAXS experiments at XCS. All movements are motorized and controlled remotely during the experiment. The jet can be monitored from different directions and with different exposure times using three microscopes. In this way, jet properties such as flow rate, jet diameter, or length can be measured *in situ* during an experiment.

In future, we will develop adapters for other nozzle designs to allow studies with other nozzle types, e.g., modified designs to use the nozzle as micro mixer for chemicals[39,40] or nozzle implementations on microfluidic chips to increase the reproducibility of the nozzle design.[41] Furthermore, a droplet-on-demand system is planned to be installed to reduce sample consumption and increase the hit-rate of X-ray pulses.[19,42] We currently integrate the setup at beamline P10 of PETRA III to routinely perform liquid jet experiments.

ACKNOWLEDGMENTS

This work was supported by the Graduate School 1355 of the Deutsche Forschungsgemeinschaft and the Hamburg Centre for Ultrafast Imaging (CUI). Use of the Linac Coherent Light Source (LCLS), SLAC National Accelerator Laboratory, is supported by the U.S. Department of Energy, Office of Science, Office of Basic Energy Sciences under Contract No. DE-AC02-76SF00515. We acknowledge the LCLS staff for preparing the x-ray beam and technical support during the beamtime. S.L. was supported by the Converging Research Center Program through the Ministry of Science, ICT and Future Planning, Korea (Grant Nos. NRF-2014M3C1A8048818 and NRF-2014M1A7A1A01030128). P.H.F. and G.B.S. were supported by the U.S. Dept. of Energy, Office of Science, Office of Basic Energy Sciences, Division of Materials Sciences and Engineering. We thank I. Rajkovic, X. Donath, and A. Menzel for support in the experiment at cSAXS of SLS.

[1]F. Lehmkühler, C. Gutt, B. Fischer, M. A. Schroer, M. Sikorski, S. Song, W. Roseker, J. Glownia, M. Chollet, S. Nelson, K. Tono, T. Katayama, M. Yabashi, T. Ishikawa, A. Robert, and G. Grübel, Sci. Rep. **4**, 5234 (2014).

[2]S. Lee, W. Roseker, C. Gutt, B. Fischer, H. Conrad, F. Lehmkühler, I. Steinke, D. Zhu, H. Lemke, M. Cammarata, D. M. Fritz, P. Wochner, M. Castro-Colin, S. O. Hruszkewycz, P. H. Fuoss, G. B. Stephenson, G. Grübel, and A. Robert, Opt. Express **21**, 24647 (2013).

[3]C. Gutt, P. Wochner, B. Fischer, H. Conrad, M. Castro-Colin, S. Lee, F. Lehmkühler, I. Steinke, M. Sprung, W. Roseker, D. Zhu, H. Lemke, S. Bogle, P. H. Fuoss, G. B. Stephenson, M. Cammarata, D. M. Fritz, A. Robert, and G. Grübel, Phys. Rev. Lett. **108**, 024801 (2012).

[4]R. Koopmann, K. Cupelli, L. Redecke, K. Nass, D. P. DePonte, T. A. White, F. Stellato, D. Rehders, M. Liang, J. Andreasson, A. Aquila, S. Bajt, M. Barthelmess, A. Barty, M. J. Bogan, C. Bostedt, S. Boutet, J. D. Bozek, C. Caleman, N. Coppola, J. Davidsson, R. B. Doak, T. Ekeberg, S. W. Epp, B. Erk, H. Fleckenstein, L. Foucar, H. Graafsma, L. Gumprecht, J. Hajdu, C. Y. Hampton, A. Hartmann, R. Hartmann, G. Hauser, H. Hirsemann, P. Holl, M. S. Hunter, S. Kassemeyer, R. A. Kirian, L. Lomb, F. R. N. C. Maia, N. Kimmel, A. V. Martin, M. Messerschmidt, C. Reich, D. Rolles, B. Rudek, A. Rudenko, I. Schlichting, J. Schulz, M. M. Seibert, R. L. Shoeman, R. G. Sierra, H. Soltau, S. Stern, L. Strueder, N. Timneanu, J. Ullrich, X. Wang, G. Weidenspointner, U. Weierstall, G. J. Williams, C. B. Wunderer, P. Fromme, J. C. H. Spence, T. Stehle, H. N. Chapman, C. Betzel, and M. Duszenko, Nat. Methods **9**, 259 (2012).

[5]S. Boutet, L. Lomb, G. J. Williams, T. R. M. Barends, A. Aquila, R. B. Doak, U. Weierstall, D. P. DePonte, J. Steinbrener, R. L. Shoeman, M. Messerschmidt, A. Barty, T. A. White, S. Kassemeyer, R. A. Kirian, M. M. Seibert, P. A. Montanez, C. Kenney, R. Herbst, P. Hart, J. Pines, G. Haller, S. M. Gruner, H. T. Philipp, M. W. Tate, M. Hromalik, L. J. Koerner, N. van Bakel, J. Morse, W. Ghonsalves, D. Arnlund, M. J. Bogan, C. Caleman, R. Fromme, C. Y. Hampton, M. S. Hunter, L. C. Johansson, G. Katona, C. Kupitz, M. Liang, A. V. Martin, K. Nass, L. Redecke, F. Stellato, N. Timneanu, D. Wang, N. A. Zatsepin, D. Schafer, J. Defever, R. Neutze, P. Fromme, J. C. H. Spence, H. N. Chapman, and I. Schlichting, Science **337**, 362 (2012).

[6]H. N. Chapman, P. Fromme, A. Barty, T. A. White, R. A. Kirian, A. Aquila, M. S. Hunter, J. Schulz, D. P. DePonte, U. Weierstall, R. B. Doak, F. R. N. C. Maia, A. V. Martin, I. Schlichting, L. Lomb, N. Coppola, R. L. Shoeman, S. W. Epp, R. Hartmann, D. Rolles, A. Rudenko, L. Foucar, N. Kimmel, G. Weidenspointner, P. Holl, M. Liang, M. Barthelmess, C. Caleman, S. Boutet, M. J. Bogan, J. Krzywinski, C. Bostedt, S. Bajt, L. Gumprecht, B. Rudek, B. Erk, C. Schmidt, A. Hoemke, C. Reich, D. Pietschner, L. Strueder, G. Hauser, H. Gorke, J. Ullrich, S. Herrmann, G. Schaller, F. Schopper, H. Soltau, K.-U. Kuehnel, M. Messerschmidt, J. D. Bozek, S. P. Hau-Riege, M. Frank, C. Y. Hampton, R. G. Sierra, D. Starodub, G. J. Williams, J. Hajdu, N. Timneanu, M. M. Seibert, J. Andreasson, A. Rocker, O. Joensson, M. Svenda, S. Stern, K. Nass, R. Andritschke, C.-D. Schroeter, F. Krasniqi, M. Bott, K. E. Schmidt, X. Wang, I. Grotjohann, J. M. Holton, T. R. M. Barends, R. Neutze, S. Marchesini, R. Fromme, S. Schorb, D. Rupp, M. Adolph, T. Gorkhover, I. Andersson, H. Hirsemann, G. Potdevin, H. Graafsma, B. Nilsson, and J. C. H. Spence, Nature **470**, 73 (2011).

[7]P. Wochner, C. Gutt, T. Autenrieth, T. Demmer, V. Bugaev, A. D. Ortiz, A. Duri, F. Zontone, G. Grübel, and H. Dosch, Proc. Natl. Acad. Sci. **106**, 11511 (2009).

[8]F. Lehmkühler, G. Grübel, and C. Gutt, J. Appl. Crystallogr. **47**, 1315 (2014).

[9]J. Carnis, W. Cha, J. Wingert, J. Kang, Z. Jiang, S. Song, M. Sikorski, A. Robert, C. Gutt, S.-W. Chen, Y. Dai, Y. Ma, H. Guo, L. B. Lurio, O. Shpyrko, S. Narayanan, M. Cui, I. Kosif, T. Emrick, T. P. Russell, H. C. Lee, C.-J. Yu, G. Grübel, S. K. Sinha, and H. Kim, Sci. Rep. **4**, 6017 (2014).
[10]G. Grübel, G. B. Stephenson, C. Gutt, H. Sinn, and T. Tschentscher, Nucl. Instrum. Methods Phys. Res., Sect. B **262**, 357 (2007).
[11]F. Lehmkühler, P. Kwasniewski, W. Roseker, B. Fischer, M. Schroer, K. Tono, T. Katayama, M. Sprung, M. Sikorski, S. Song, J. Glownia, M. Chollet, S. Nelson, A. Robert, C. Gutt, M. Yabashi, T. Ishikawa, and G. Grübel, Sci. Rep. **5**, 17193 (2015).
[12]R. Owen, E. Rudino-Pinera, and E. Garman, Proc. Natl. Acad. Sci. **103**, 4912 (2006).
[13]C. Riekel, J. Synchrotron Radiat. **11**, 4 (2004).
[14]K. Tono, E. Nango, M. Sugahara, C. Song, J. Park, T. Tanaka, R. Tanaka, Y. Joti, T. Kameshima, S. Ono, T. Hatsui, E. Mizohata, M. Suzuki, T. Shimamura, Y. Tanaka, S. Iwata, and M. Yabashi, J. Synchrotron Radiat. **22**, 532 (2014).
[15]C. Song, K. Tono, J. Park, T. Ebisu, S. Kim, H. Shimada, S. Kim, M. Gallagher-Jones, D. Nam, T. Sato, T. Togashi, K. Ogawa, Y. Joti, T. Kameshima, S. Ono, T. Hatsui, S. Iwata, M. Yabashi, and T. Ishikawa, J. Appl. Crystallogr. **47**, 188 (2014).
[16]U. Weierstall, J. Spence, and R. Doak, Rev. Sci. Instrum. **83**, 035108 (2012).
[17]J. Spence, U. Weierstall, and H. Chapman, Rep. Prog. Phys. **75**, 102601 (2012).
[18]L. Strüder, S. Eppa, D. Rolles, R. Hartmann, P. Holl, G. Lutz, H. Soltau, R. Eckart, C. Reich, K. Heinzinger, C. Thamm, A. Rudenko, F. Krasniqi, K.-U. Kuehnel, C. Bauer, C.-D. Schroeter, R. Moshammer, S. Techert, D. Miessner, M. Porro, O. Haelker, N. Meidinger, N. Kimmel, R. Andritschke, F. Schopper, G. Weidenspointner, A. Ziegler, D. Pietschner, S. Herrmann, U. Pietsch, A. Walenta, W. Leitenberger, C. Bostedt, T. Moeller, D. Rupp, M. Adolph, H. Graafsma, H. Hirsemann, K. Gaertner, R. Richter, L. Foucar, R. L. Shoeman, I. Schlichting, and J. Ullrich, Nucl. Instrum. Methods Phys. Res., Sect. A **614**, 483 (2010).
[19]U. Weierstall, Philos. Trans. R. Soc., B **369**, 20130337 (2014).
[20]D. P. DePonte, U. Weierstall, K. Schmidt, J. Warner, D. Starodub, J. C. H. Spence, and R. B. Doak, J. Phys. D: Appl. Phys. **41**, 195505 (2008).
[21]A. J. Acero, C. Ferrera, J. M. Montanero, and A. M. Gañán-Calvo, J. Micromech. Microeng. **22**, 065011 (2012).
[22]D. P. DePonte, R. B. Doak, M. Hunter, L. Z., U. Weierstall, and J. C. H. Spence, Micron **40**, 507 (2009).
[23]A. Gañán-Calvo, Phys. Rev. Lett. **80**, 285 (1998).
[24]A. Gañán-Calvo, M. Herrada, and J. Montanero, Phys. Fluid **26**, 061701 (2014).
[25]R. Alonso-Mori, C. Caronna, M. Chollet, R. Curtis, D. S. Damiani, J. Defever, Y. Feng, D. L. Flath, J. M. Glownia, S. Lee, H. T. Lemke, S. Nelson, E. Bong, M. Sikorski, S. Song, V. Srinivasan, D. Stefanescu, D. Zhu, and A. Robert, J. Synchrotron Radiat. **22**, 508 (2015).
[26]S. Send, A. Abboud, R. Hartmann, M. Huth, W. Leitenberger, N. Pashniak, J. Schmidt, L. Strüder, and U. Pietsch, Nucl. Instrum. Methods Phys. Res., Sect. A **711**, 132 (2013).
[27]A. Abboud, S. Send, N. Pashniak, W. Leitenberger, S. Ihle, M. Huth, R. Hartmann, L. Strüder, and U. Pietsch, J. Instrum. **8**, P05005 (2013).
[28]J. Amann, W. Berg, V. Blank, F.-J. Decker, Y. Ding, P. Emma, Y. Feng, J. Frisch, D. Fritz, J. Hastings, Z. Huang, J. Krzywinski, R. Lindberg, H. Loos, A. Lutman, H.-D. Nuhn, D. Ratner, J. Rzepiela, D. Shu, Y. Shvyd'ko, S. Spampinati, S. Stoupin, S. Terentyev, E. Trakhtenberg, D. Walz, J. Welch, J. Wu, A. Zholents, and D. Zhu, Nat. Photon. **6**, 693 (2012).
[29]M. Ozaki, S. Kratohvil, and E. Matijevic, J. Colloid Interface Sci. **102**, 146 (1984).
[30]R. L. Blake, R. E. Hessevick, T. Zoltai, and L. W. Finger, Am. Mineral. **51**, 123 (1966).
[31]D. Gunes, R. Scirocco, J. Mewis, and J. Vermant, J. Non-Newtonian Fluid Mech. **155**, 39 (2008).
[32]R. Reitz and F. Bracco, "Mechanisms of breakup of round liquid jets," in *The Encyclopedia of Fluid Mechanics* (Gulf, Housten, 1986).
[33]J. Montanero, M. Herrada, C. Ferrera, E. Vega, and A. Gañán-Calvo, Phys. Fluids **23**, 122103 (2011).
[34]W. Leitenberger, R. Hartmann, U. Pietsch, R. Andritschke, I. Starke, and L. Strüder, J. Synchrotron Radiat. **15**, 449 (2008).
[35]F. Livet, F. Bley, J. Mainville, R. Caudron, S. Mochrie, E. Geissler, G. Dolino, D. Abernathy, G. Grübel, and M. Sutton, Nucl. Instrum. Methods Phys. Res., Sect. A **451**, 596 (2000).
[36]S. O. Hruszkewycz, M. Sutton, P. H. Fuoss, B. Adams, S. Rosenkranz, K. F. Ludwig, Jr., W. Roseker, D. Fritz, M. Cammarata, D. Zhu, S. Lee, H. Lemke, C. Gutt, A. Robert, G. Grübel, and G. B. Stephenson, Phys. Rev. Lett. **109**, 185502 (2012).
[37]G. Hura, J. Sorenson, R. Glaeser, and T. Head-Gordon, J. Chem. Phys. **113**, 9140 (2000).
[38]M. Trebbin, D. Steinhauser, J. Perlich, A. Buffet, S. Roth, W. Zimmermann, J. Thiele, and S. Förster, Proc. Natl. Acad. Sci. **110**, 6706 (2013).
[39]A. Wang, U. Weierstall, L. Pollack, and J. Spence, J. Synchrotron Radiat. **21**, 1 (2014).
[40]A. Gañán-Calvo, C. Ferrera, M. Torregrosa, M. A. Herrada, and M. Marchand, Microfluid. Nanofluid. **11**, 65 (2011).
[41]M. Trebbin, K. Krüger, D. DePonte, S. V. Roth, H. N. Chapman, and S. Foerster, Lab Chip **14**, 1733 (2014).
[42]J. A. Sellberg, C. Huang, T. A. McQueen, N. D. Loh, H. Laksmono, D. Schlesinger, R. G. Sierra, D. Nordlund, C. Y. Hampton, D. Starodub, D. P. DePonte, M. Beye, C. Chen, A. V. Martin, A. Barty, K. T. Wikfeldt, T. M. Weiss, C. Caronna, J. Feldkamp, L. B. Skinner, M. M. Seibert, M. Messerschmidt, G. J. Williams, S. Boutet, L. G. M. Pettersson, M. J. Bogan, and A. Nilsson, Nature **510**, 381 (2014).